

# Exploring Wrong Sign Scenarios in the Yukawa-Aligned 2HDM

---

**Shinya Kanemura, Tanmoy Mondal and Kei Yagyu**

*Department of Physics, Osaka University, Toyonaka, Osaka 560-0043, Japan*

*E-mail:* [kanemu@het.phys.sci.osaka-u.ac.jp](mailto:kanemu@het.phys.sci.osaka-u.ac.jp),  
[tanmoy@het.phys.sci.osaka-u.ac.jp](mailto:tanmoy@het.phys.sci.osaka-u.ac.jp),  
[yagyu@het.phys.sci.osaka-u.ac.jp](mailto:yagyu@het.phys.sci.osaka-u.ac.jp)

**ABSTRACT:** We discuss scenarios with wrong-sign (WS) Yukawa couplings for the discovered Higgs boson in the Yukawa-aligned two Higgs doublet model. In the WS scenario, Yukawa couplings for down-type quarks and/or charged leptons have an opposite sign as compared to those of the Higgs boson in the standard model, which can be consistent with current flavor data and the Higgs signal strengths. The phenomenology of additional Higgs bosons in such a scenario can be significantly different from that with right-sign Yukawa couplings, mainly due to a larger Higgs boson mixing to be required in the wrong-sign case. We show the parameter space which is excluded or explored by direct searches for the additional Higgs bosons at the current and high-luminosity LHC under the constraints from perturbative unitarity and vacuum stability. In particular, we find that most of the parameter space is explored in the WS scenario with the Type-X (lepton specific) Yukawa interaction which is a special case of the Yukawa alignment realized by imposing a softly-broken  $\mathbb{Z}_2$  symmetry. We propose that multi-Higgs events from pair productions of the additional Higgs bosons can be the smoking gun signature to probe the WS scenario, and give the expected number of events at the high-luminosity LHC.

---

## Contents

|          |   |           |
|----------|---|-----------|
| <b>1</b> | <b>Introduction</b>   | <b>1</b>  |
| <b>2</b> | <b>WS Yukawa Couplings in 2HDMs</b>                               | <b>3</b>  |
| <b>3</b> | <b>Constraints on WS Yukawa Couplings</b>                         | <b>7</b>  |
| 3.1      | Higgs Signal Strengths  | 7         |
| 3.2      | Theoretical Constraints   | 9         |
| 3.3      | Flavor Constraints  | 10        |
| <b>4</b> | <b>Decays of Additional Higgs Bosons in RS &amp; WS Scenarios</b> | <b>12</b> |
| <b>5</b> | <b>Limits from Current LHC and HL-LHC</b>                         | <b>15</b> |
| <b>6</b> | <b>Multi-Higgs Signatures in the WS Scenario</b>                  | <b>17</b> |
| <b>7</b> | <b>Conclusion</b>   | <b>20</b> |
| <b>A</b> | <b>Higgs measurement data</b>                                     | <b>20</b> |
| <b>B</b> | <b>Number of events for two Higgs final states</b>                | <b>21</b> |

---

## 1 Introduction

Current LHC data show that the properties of the discovered Higgs boson are consistent with those in the Standard Model (SM) [1, 2]. On the other hand, the Higgs sector is extended from the minimal form with one isospin doublet field in various new physics models, which are motivated to explain phenomena beyond the SM, such as neutrino oscillations, dark matter and baryon asymmetry of the Universe. In an extended Higgs sector, the so-called Higgs alignment is approximately required from the above situation, where one of the mass eigenstates of neutral Higgs bosons with a mass of 125 GeV ( $h$ ) coincides with a component of the Higgs doublet field whose vacuum expectation value (VEV) takes the SM value. In the Higgs alignment limit, all the Higgs boson couplings with SM particles take the same values as those in the SM at the tree level. Thus, the Higgs alignment is now getting quite important in models with extended Higgs sectors to accommodate the current situation.

The Higgs alignment is realized by taking the decoupling limit, in which all the masses of additional Higgs bosons are taken to be infinity. This, however, is

essentially the same as the SM-limit, so that desired properties of extended Higgs sectors, e.g., explaining unsolved phenomena and testability at collider experiments, must be spoiled. There is an alternative and attractive way to realize the Higgs alignment, i.e., the so-called alignment without decoupling, in which mixing of  $h$  with the other neutral states vanishes. In this case, masses of additional Higgs bosons can be at the electroweak scale, while couplings of  $h$  are kept at the SM values. In practice, we do not need to demand the exact Higgs alignment because the observed  $h$  couplings, defined by the  $\kappa$ -scheme [3], include typically of order 10% uncertainties. In the nearly aligned scenario, the Higgs boson coupling to the weak bosons takes a similar value to the SM one. In contrast, particularly in models with multi-Higgs doublets, Yukawa couplings can have either right-sign (RS) or wrong-sign (WS) with a similar magnitude to those in the SM. In the RS (WS) scenario, the sign of Yukawa couplings is the same (opposite) as compared to the corresponding SM ones. Thus, measurement of the “sign”<sup>1</sup> of Yukawa couplings is crucial to understand the structure of the Higgs sector.

The WS scenario, having WS Yukawa couplings, has been studied earlier in Refs. [4–13] in the Type-II two Higgs doublet model (2HDM), where Yukawa couplings for down-type quarks and charged leptons are WS. In this case, most of the parameter space has already been excluded by the constraints from  $B$  physics data, the Higgs signal strength and direct searches for additional Higgs bosons [11]. The WS scenario has also been discussed in the Type-X 2HDM based on the motivation to explain the anomaly of the muon anomalous magnetic moment  $(g-2)_\mu$  [14–16], where a smaller mass of the CP-odd Higgs boson ( $A$ ) than half of the mass of  $h$  is required. See also Refs. [17, 18] (Ref. [19]) for the discussion of the  $(g-2)_\mu$  anomaly in the Type-X 2HDM (Yukawa aligned 2HDM defined below) with the light CP-odd Higgs boson. Although such a light  $A$  can easily be excluded by the constraint  $\text{BR}(h \rightarrow AA) \lesssim 5\%$  with leptonic decays of  $A$  given at the LHC [20–25], the WS scenario in the Type-X 2HDM allows to take the  $hAA$  coupling to be negligibly small [14–16, 26–29]. Unlike the Type-II 2HDM, the phenomenology of the additional Higgs bosons has not intensively been discussed, since gluon fusion production is inefficient due to the significant suppression of quark Yukawa couplings in the Type-X 2HDM.

So far, the WS scenario has been studied in the 2HDMs with a softly-broken  $\mathbb{Z}_2$  symmetry, for e.g., the Type-II and Type-X 2HDMs as aforementioned. In this work, we focus on the WS scenario in Yukawa aligned 2HDMs (A2HDMs), where flavor changing neutral currents (FCNCs) via Higgs boson exchanges at the tree level vanish due to the assumption that one of the Yukawa matrices for each charged fermion is proportional to the other [30].

---

<sup>1</sup>To be more precise, we here mean the relative sign between a fermion mass and a coefficient of a Higgs-fermion-antifermion vertex.

The A2HDM provides additional CP-violating (CPV) phases in Yukawa interactions and the Higgs potential, which do not appear in the 2HDMs with the  $\mathbb{Z}_2$  symmetry. Recently, it has been found that severe constraints from electric dipole moments can be avoided due to destructive interferences among fermion and scalar loop diagrams [31], and the testability of the CPV phases at future lepton colliders have been discussed in Ref. [32]. Furthermore, in Refs. [33, 34], it has been clarified that the observed baryon asymmetry of the Universe can be explained based on the electroweak baryogenesis scenario in the CPV A2HDM.

In this paper, we investigate the CP-conserving A2HDM<sup>2</sup> with WS Yukawa couplings under the constraints coming from perturbative unitarity [36–40], vacuum stability [41–43], flavor data, the Higgs signal strength and the direct searches at the LHC. As a special case of the A2HDM, we also explore the Type-X 2HDM without requiring the light  $A$ , which has been studied in the previous works mentioned above. We show that in the WS scenario, bosonic decay channels of the additional Higgs bosons, such as  $H \rightarrow hh/WW/ZZ$ ,  $A \rightarrow Zh$ ,  $H^\pm \rightarrow W^\pm h$ <sup>3</sup> tend to be more important as compared with those in the RS scenario. We find that the direct searches for additional Higgs bosons at the High-Luminosity LHC (HL-LHC) can explore most of the parameter space in the Type-X scenario, which is allowed by the theoretical constraints. In addition, in the A2HDM, the HL-LHC can explore a large portion of the parameter space, up to around 1 TeV for the masses of additional Higgs bosons. We propose that multi-Higgs signatures from pair productions of the additional Higgs boson can be the smoking gun to probe the WS scenario and give the expected number of events at the HL-LHC.

This paper is organized as follows: We begin with a brief discussion of the A2HDM and the structure of Yukawa interactions in Sec. 2. Next, in Sec. 3, we discuss various theoretical and experimental constraints and their impact on the WS scenario. To distinguish the WS and RS scenarios, in Sec. 4, we compare the branching ratios of additional neutral Higgs bosons. Sec. 5 shows the current limit on the parameter space in the A2HDM from direct searches at the LHC Run-II experiment, In Sec. 6, we discuss the prospect of looking for the WS scenarios via multi-Higgs searches at the HL-LHC. We then conclude our findings in Sec. 7.

## 2 WS Yukawa Couplings in 2HDMs

The 2HDM consists of two isospin scalar doublets  $\Phi_1$  and  $\Phi_2$  with hypercharge  $Y = 1/2$ . For reviews of the 2HDM, see e.g., [47–49]. Throughout this paper, we neglect new CPV phases in the Higgs sector for simplicity.

<sup>2</sup>See Ref. [35] for a recent global fit in the A2HDM.

<sup>3</sup>See Refs. [44], [45] and [46] for the recent study on electroweak radiative corrections to the  $H$ ,  $A$  and  $H^\pm$  decays in the 2HDMs with the  $\mathbb{Z}_2$  symmetry, respectively.

We first define the Higgs basis [50, 51] expressed as

$$\begin{pmatrix} \Phi_1 \\ \Phi_2 \end{pmatrix} = \begin{pmatrix} 1 & 0 \\ 0 & e^{i\xi} \end{pmatrix} \begin{pmatrix} \cos\beta & -\sin\beta \\ \sin\beta & \cos\beta \end{pmatrix} \begin{pmatrix} \Phi \\ \Phi' \end{pmatrix}, \quad (2.1)$$

where  $\xi$  is the relative phase of two VEVs. In the Higgs basis, the doublets are parametrized as,

$$\Phi = \begin{pmatrix} G^\pm \\ \frac{1}{\sqrt{2}}(v + S_1 + iG^0) \end{pmatrix}, \quad \Phi' = \begin{pmatrix} H^\pm \\ \frac{1}{\sqrt{2}}(S_2 + iA) \end{pmatrix}, \quad (2.2)$$

where only  $\Phi$  contains the VEV  $v \simeq 246$  GeV. In the above expression,  $G^\pm$  ( $G^0$ ) are the Nambu-Goldstone bosons which are absorbed into the longitudinal component of the  $W^\pm$  ( $Z$ ) bosons, while  $H^\pm$ ,  $A$  and  $S_{1,2}$  are respectively the physical singly-charged, CP-odd and CP-even Higgs states.

The general scalar potential is given by,

$$\begin{aligned} V = & m^2|\Phi|^2 + M^2|\Phi'|^2 - (\mu^2\Phi^\dagger\Phi' + \text{h.c.}) + \frac{\Lambda_1}{2}|\Phi|^4 + \frac{\Lambda_2}{2}|\Phi'|^4 + \Lambda_3|\Phi|^2|\Phi'|^2 + \Lambda_4|\Phi^\dagger\Phi'|^2 \\ & + \left[ \frac{\Lambda_5}{2}(\Phi^\dagger\Phi') + \Lambda_6|\Phi|^2 + \Lambda_7|\Phi'|^2 \right] (\Phi^\dagger\Phi') + \text{h.c.}, \end{aligned} \quad (2.3)$$

where  $\mu^2$  and  $\Lambda_{5,6,7}$  are assumed to be real. Minimization of the potential gives the following tadpole solutions,

$$m^2 = -\frac{\Lambda_1}{2}v^2 \quad , \quad \mu^2 = \frac{\Lambda_6}{2}v^2. \quad (2.4)$$

To obtain the mass eigenstates of the CP-even states, we introduce the mixing angle  $\beta - \alpha$  as <sup>4</sup>,

$$\begin{pmatrix} H \\ h \end{pmatrix} = \begin{pmatrix} \cos(\beta - \alpha) & -\sin(\beta - \alpha) \\ \sin(\beta - \alpha) & \cos(\beta - \alpha) \end{pmatrix} \begin{pmatrix} S_1 \\ S_2 \end{pmatrix}, \quad (2.5)$$

where we can identify  $h$  with the discovered Higgs boson with the mass of 125 GeV. Some of the parameters in the potential can be rewritten in terms of masses and

---

<sup>4</sup>In the general 2HDM, the parameter  $\beta$  does not have physical impacts, but here we express the mixing angle to be  $\beta - \alpha$  as the analogy to the 2HDMs with the softly-broken  $Z_2$  symmetry.

mixing angles as follows:

$$\Lambda_1 = \frac{\sin^2(\beta - \alpha)M_h^2 + \cos^2(\beta - \alpha)M_H^2}{v^2}, \quad (2.6)$$

$$\Lambda_3 = \frac{2(M_{H^\pm}^2 - M^2)}{v^2}, \quad (2.7)$$

$$\Lambda_4 = \frac{\cos^2(\beta - \alpha)M_h^2 + \sin^2(\beta - \alpha)M_H^2 + M_A^2 - 2M_{H^\pm}^2}{v^2}, \quad (2.8)$$

$$\Lambda_5 = \frac{\cos^2(\beta - \alpha)M_h^2 + \sin^2(\beta - \alpha)M_H^2 - M_A^2}{v^2}, \quad (2.9)$$

$$\Lambda_6 = \frac{\sin(\beta - \alpha) \cos(\beta - \alpha) (M_h^2 - M_H^2)}{v^2}. \quad (2.10)$$

For our phenomenological analysis, we choose the following set of input parameters:

$$v, M_h, M_H, M_A, M_{H^\pm}, \Lambda_2, \Lambda_3, \Lambda_7, \text{ and } \cos(\beta - \alpha), \quad (2.11)$$

where  $v$  and  $M_h$  are fixed to be about 246 GeV and 125 GeV, respectively.

We note in passing that in the 2HDMs with the  $\mathbb{Z}_2$  symmetry, two of seven quartic couplings, i.e., the coefficients of  $|\Phi_1|^2(\Phi_1\Phi_2^\dagger)$  and  $|\Phi_2|^2(\Phi_1\Phi_2^\dagger)$  in the general basis, are forbidden. As a result, two quartic couplings in the Higgs basis are written by the other parameters. For instance,  $\Lambda_2$  and  $\Lambda_7$  are written as

$$\Lambda_2 = \Lambda_1 \left( 3 - \frac{2}{\sin^2 2\beta} \right) + 2(\Lambda_3 + \Lambda_4 + \Lambda_5) \cot^2 2\beta - \frac{2\Lambda_6}{\sin^3 2\beta} (\cos 2\beta + \cos 6\beta), \quad (2.12)$$

$$\Lambda_7 = \Lambda_6(1 - 2 \cot^2 2\beta) + (\Lambda_3 + \Lambda_4 + \Lambda_5 - \Lambda_1) \cot 2\beta. \quad (2.13)$$

These relations turn out to be important when we consider the constraint on the parameter space from perturbative unitarity as it will be discussed in Sec. 3.

The Yukawa interactions are generally expressed in the mass eigenstates of fermions as,

$$\begin{aligned} \mathcal{L}_Y = & -\bar{Q}_L^d \left( \frac{\sqrt{2}M_d}{v} \Phi + \rho_d \Phi' \right) d_R - \bar{Q}_L^u \left( \frac{\sqrt{2}M_u}{v} \tilde{\Phi} + \rho_u \tilde{\Phi}' \right) u_R \\ & - \bar{L}_L \left( \frac{\sqrt{2}M_e}{v} \Phi + \rho_e \Phi' \right) e_R + \text{h.c.}, \end{aligned} \quad (2.14)$$

where  $\tilde{\Phi} = i\sigma_2\Phi^*$ ,  $Q_L^u = (u_L, V_{\text{CKM}}d_L)^T$ ,  $Q_L^d = (V_{\text{CKM}}^\dagger u_L, d_L)^T$  and  $L_L = (\nu_L, e_L)$  with  $V_{\text{CKM}}$  being the Cabibbo-Kobayashi-Maskawa matrix. In the above expression,  $M_f$  ( $f = u, d, e$ ) are the diagonal mass matrices for charged fermions, and  $\rho_f$  are arbitrary  $3 \times 3$  complex matrices which can cause FCNCs mediated by the Higgs bosons at

tree level. In order to avoid such FCNCs, we impose the Yukawa-alignment [30] in the flavor space: <sup>5</sup>

$$\rho_{d,e} = \sqrt{2}\zeta_{d,e} \frac{M_{d,e}}{v} \quad \text{and} \quad \rho_u = \sqrt{2}\zeta_u^* \frac{M_u}{v}. \quad (2.15)$$

We call  $\zeta_f$  the alignment parameters which are generally complex-valued. After applying the aforementioned alignment condition, we obtain the Yukawa interaction terms for the physical Higgs bosons as follows:

$$\begin{aligned} \mathcal{L}_Y^{\text{int}} = & - \sum_{f=u,d,e} \bar{f}_L \frac{M_f}{v} f_R (\kappa_f h + \kappa_f^H H + i \kappa_f^A A) \\ & - \frac{\sqrt{2}}{v} H^+ (\zeta_d \bar{u}_L V_{\text{CKM}} M_d d_R - \zeta_u \bar{u}_R M_u^\dagger V_{\text{CKM}} d_L + \zeta_e \bar{\nu}_L M_e e_R) + \text{h.c.} \end{aligned} \quad (2.16)$$

The Yukawa coupling modifiers are given by

$$\begin{aligned} \kappa_f &= \sin(\beta - \alpha) + \zeta_f \cos(\beta - \alpha), \\ \kappa_f^H &= \cos(\beta - \alpha) - \zeta_f \sin(\beta - \alpha), \quad \text{and} \quad \kappa_f^A = -2I_{3f}\zeta_f, \end{aligned} \quad (2.17)$$

with  $I_{3f}$  being the third component of the isospin.

Apart from the Yukawa alignment, the Higgs-mediated FCNCs can also be forbidden by imposing the softly-broken  $\mathbb{Z}_2$  symmetry, which restricts each type of the right-handed fermions to couple to only one of  $\Phi_1$  and  $\Phi_2$ . Depending on the  $\mathbb{Z}_2$  charge assignment, four different types of Yukawa interactions are possible [53–55]. The  $\mathbb{Z}_2$  symmetric scenarios are the special case of the A2HDMS, i.e., the alignment parameters  $\zeta_f$  are expressed by the single parameter  $\beta$  as

$$\begin{aligned} \zeta_u &= \zeta_d = \zeta_e = 1/\tan\beta \quad (\text{Type-I}), \\ \zeta_u &= 1/\tan\beta \quad \text{and} \quad \zeta_d = \zeta_e = -\tan\beta \quad (\text{Type-II}), \\ \zeta_u &= \zeta_d = 1/\tan\beta \quad \text{and} \quad \zeta_e = -\tan\beta \quad (\text{Type-X}), \\ \zeta_u &= \zeta_e = 1/\tan\beta \quad \text{and} \quad \zeta_d = -\tan\beta \quad (\text{Type-Y}). \end{aligned} \quad (2.18)$$

The scaling factor  $\kappa_f$  in Eq. (2.16) parameterizes the deviation in the Yukawa couplings from the SM values. Similarly, we can define  $\kappa_V = \sin(\beta - \alpha)$  for the weak bosons. Current measurements restrict  $\kappa$  values close to unity. From Eq. (2.17), we see that  $\kappa_f$  stays close to the SM values when  $\sin(\beta - \alpha) \simeq 1$  with  $|\zeta_f \cos(\beta - \alpha)| \ll 1$ , which is called the RS scenario. It is also possible to have  $\kappa_f = -1$  when

$$\zeta_f = -\frac{1}{\cos(\beta - \alpha)} [1 + \sin(\beta - \alpha)], \quad (2.19)$$

---

<sup>5</sup>The Yukawa alignment condition is not protected by a symmetry, so that it is generally broken at loop levels. The deviation from the alignment condition has been studied by using the renormalization group equations in Refs. [31, 52], and found that the size of the deviation is typically quite small as this should be proportional to small off-diagonal components of the CKM matrix. Throughout this paper, we neglect such a loop effect on the Yukawa couplings.

which is approximately expressed as  $\zeta_f \sim -2/\cos(\beta - \alpha)$  for  $\sin(\beta - \alpha) \simeq 1$ . We call the limit defined in Eq. (2.19) as the WS limit for the Yukawa coupling<sup>6</sup> In the following, we discuss the parameter space which can give rise to the approximate WS limit, and study relevant constraints on such a parameter space.

### 3 Constraints on WS Yukawa Couplings

#### 3.1 Higgs Signal Strengths

We discuss whether WS scenarios are consistent with the measurement of the Higgs signal strength<sup>7</sup>. First of all, we consider the WS for the top Yukawa coupling. In this case, the decay rate of the  $h \rightarrow \gamma\gamma$  process is significantly enhanced, because the destructive interference between the  $W$  boson and top quark loops in the SM alters constructive. In Fig. 1, we show the contour plot of  $\kappa_\gamma \equiv \sqrt{\Gamma(h \rightarrow \gamma\gamma)/\Gamma(h_{\text{SM}} \rightarrow \gamma\gamma)}$  as a function of  $\kappa_V$  and  $\kappa_t (= \kappa_u)$ . It is evident that  $\kappa_V$  needs to deviate substantially from unity to accommodate the WS top Yukawa, i.e.,  $\kappa_V \lesssim 0.8$  for  $\kappa_t = -1$  in order to satisfy the constraint  $0.9 < \kappa_\gamma < 1.2$  at 95% CL provided by the LHC [1]. Such a large deviation in  $\kappa_V$  has already been excluded by the LHC data [1, 2], so that the scenario with the WS top Yukawa is now highly disfavored. We thus consider the WS scenario in Yukawa couplings for down-type quarks and/or charged leptons in the following discussion.

We apply a  $\chi^2$  analysis to constrain the parameter space based on the data shown in Appendix A. We scan the relevant parameters  $\sin(\beta - \alpha)$ ,  $\zeta_u$ ,  $\zeta_d$  and  $\zeta_e$ , and calculate  $\Delta\chi^2$  for each scanned point. We find that the minimum of  $\chi^2$  is given at  $\kappa_V = 1.02$ ,  $\kappa_u = 1.01$ ,  $\kappa_d = 1.03$  and  $\kappa_e = 0.96$ . The parameter space allowed at  $2\sigma$  level is shown in Fig. 2. We see that two separate regions satisfy the Higgs data. The central part corresponds to the RS scenario, while the bands in the top-left and bottom-right correspond to the WS scenario, where  $\zeta_{d/e} \cos(\beta - \alpha) \simeq -2$  is satisfied. We note that in the  $\mathbb{Z}_2$  symmetric 2HDMs, the WS scenario is possible only for  $\cos(\beta - \alpha) > 0$  because of the structure of the Yukawa coupling given in Eq. (2.18).

Fig. 3 shows the parameter space allowed by the constraints from the Higgs signal strength within  $2\sigma$  on the  $\zeta_e$ - $\zeta_d$  plane for a fixed value of  $\cos(\beta - \alpha)$  and  $\zeta_u$ . In this figure, the dotted curve shows the case in the Type-II (left) and Type-X (right) 2HDM. We see that small deviations from these 2HDMs shown by the ellipses are allowed, and these are realized in the A2HDM.

It is worth mentioning here that the WS scenario typically requires large  $\tan\beta$  in the 2HDMs with the  $\mathbb{Z}_2$  symmetry, which gives  $\kappa_d = \kappa_e = -1$  ( $\kappa_e = -1$ ) and

<sup>6</sup>Notice here that by substituting  $\zeta_f = -\tan\beta$  in Eq. (2.19) we obtain the WS limit  $\sin(\beta + \alpha) = 1$  [5] for the  $\mathbb{Z}_2$  symmetric case.

<sup>7</sup>Throughout this subsection, we take  $M_{H^\pm} = 200$  GeV, and  $\Lambda_3$  is fixed such that  $\Lambda_2 = 4\pi$  is realized for the calculation of the charged Higgs boson loop in the  $h \rightarrow \gamma\gamma$  decay. Such an effect on the  $\chi^2$  analysis is not significant.



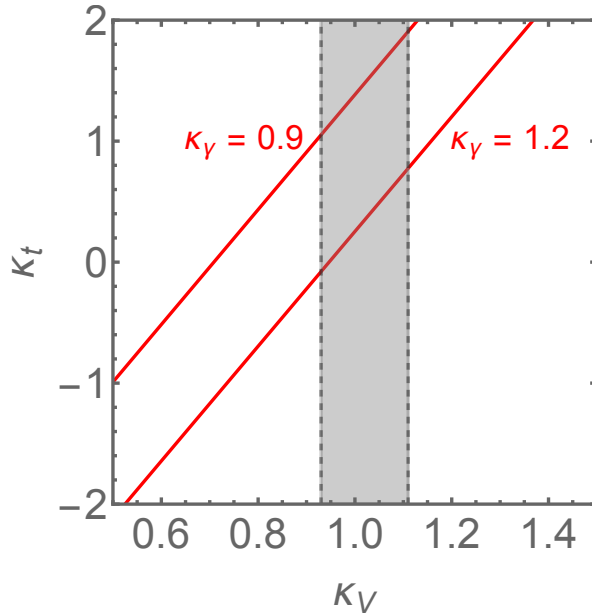


**Figure 1.** Contour of  $2\sigma$  allowed region of  $\kappa_\gamma$  as a function of  $\kappa_V$  and  $\kappa_t (= \kappa_u)$ . Shaded regions are allowed at 95% CL by the current measurement of  $\kappa_V$  at the LHC.

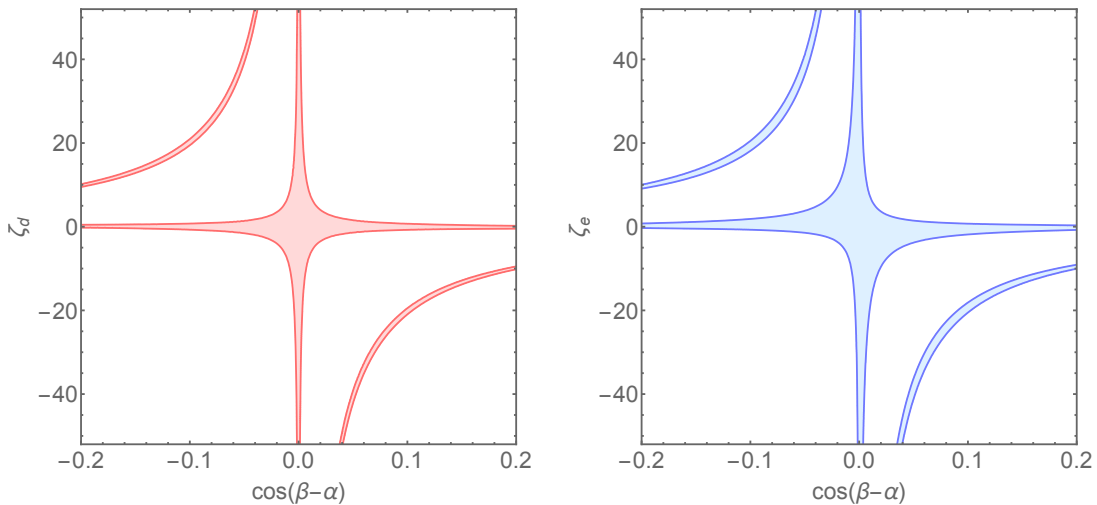


**Figure 2.** Shaded regions are the parameter space allowed at  $2\sigma$  level from the measurements of the Higgs signal strength at the LHC. We show the allowed region on the  $\cos(\beta - \alpha)$ - $\zeta_d$  (left panel) and  $\cos(\beta - \alpha)$ - $\zeta_e$  (right panel) plane. We fixed  $M_{H^\pm} = 200$  GeV,  $\Lambda_3$  is fixed such that  $\Lambda_2 = 4\pi$ , and all remaining parameters were scanned.

$\kappa_u \simeq \kappa_V$  ( $\kappa_u \simeq \kappa_d \simeq \kappa_V$ ) in the WS Type-II (WS Type-X) 2HDM. On the other hand, in the A2HDM, even if we impose the WS condition for, e.g.,  $\kappa_e$ , the  $\kappa_u$ ,  $\kappa_d$  and  $\kappa_V$  parameters can differently deviate from unity because these are controlled by

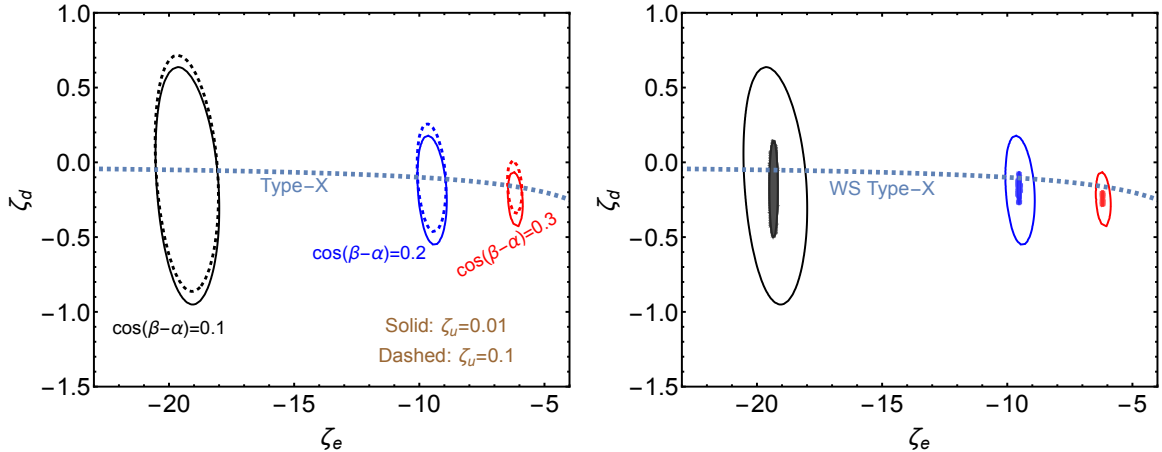


**Figure 3.** Regions inside the ellipses are allowed by the measurement of the Higgs signal strength at  $2\sigma$  level on the  $\zeta_d$ - $\zeta_e$  plane for fixed values of  $\cos(\beta - \alpha)$  and  $\zeta_u = 0.1$ . The filled ellipses in the right panel shows projected allowed region at the HL-LHC. The projected uncertainties are taken from [56]. The dashed curve shows the case realized in the Type-II (Type-X) 2HDM in the left (right) panel.

$\zeta_u$ ,  $\zeta_d$  and  $\sin(\beta - \alpha)$ , respectively. Therefore, by measuring the pattern of deviations in the  $h$  couplings from the SM predictions, we can distinguish the WS scenario in the A2HDM from that in the  $\mathbb{Z}_2$  symmetric 2HDMs, see also Ref. [57, 58] for the model discrimination by “fingerprinting” the  $h$  couplings.

### 3.2 Theoretical Constraints

The quartic couplings are constrained by the requirement of vacuum stability of the scalar potential and perturbative unitarity of the  $S$ -matrix.

The condition of the vacuum stability, i.e., bounded from below in any direction with large field values, is given by [41–43],

$$\begin{aligned} \Lambda_1 \geq 0, \quad \Lambda_2 \geq 0, \quad \sqrt{\Lambda_1 \Lambda_2} + \Lambda_3 \geq 0, \quad \sqrt{\Lambda_1 \Lambda_2} + \Lambda_3 + \Lambda_4 - |\Lambda_5| \geq 0 \\ \frac{1}{2}(\Lambda_1 + \Lambda_2) + \Lambda_3 + \Lambda_4 + \Lambda_5 - 2|\Lambda_6 + \Lambda_7| \geq 0. \end{aligned} \quad (3.1)$$

For the perturbative unitarity, we consider 2-body to 2-body elastic scatterings for bosonic states in the high-energy limit. The analytic expressions for the eigenvalues of the  $s$ -wave amplitude matrix have been found in the  $\mathbb{Z}_2$  symmetric case in Refs. [36–38]. In the general 2HDM, the  $s$ -wave amplitude matrix is expressed by a block diagonal form with maximally  $4 \times 4$  block matrices [39, 40] which can be numerically diagonalized. The limit on the masses due to vacuum stability, unitarity and perturbativity ( $|\Lambda_i| < 4\pi$ ) is shown in Fig. 4. For simplicity, we here assume degenerate masses of the additional Higgs bosons, i.e.,  $M_\Phi \equiv M_{H^\pm} (= M_A = M_H)$ .

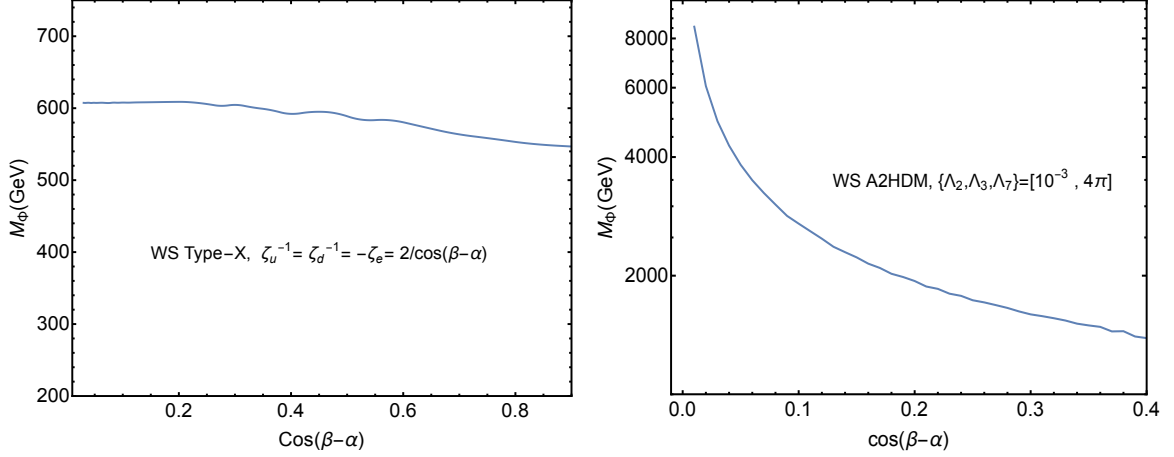


**Figure 4.** Upper limit on the mass of the additional Higgs bosons  $M_\Phi = M_{H^\pm} (= M_A = M_H)$  from the perturbative unitarity and the vacuum stability as a function of  $\cos(\beta - \alpha)$  in the 2HDMs with the softly-broken  $\mathbb{Z}_2$  symmetry (left) and the A2HDM (right).

All the other relevant parameters are scanned with a sufficiently large range to maximize the upper limit on  $M_\Phi$ . The left panel shows the result in the  $\mathbb{Z}_2$  symmetric case with the exact WS condition, i.e.,  $\tan \beta = 2/\cos(\beta - \alpha)$ , where large values of  $\tan \beta$  are required for the case with the nearly Higgs alignment  $\cos(\beta - \alpha) \simeq 0$ . In such a case with  $\tan \beta \gg 1$  and the nearly Higgs alignment  $\cos(\beta - \alpha) \sim 0$ , the  $\Lambda_2$  parameter can be expressed by using Eq. (2.12) as

$$\Lambda_2 \simeq \frac{\tan^2 \beta}{4v^2} \left[ (M_h^2 - M_H^2) \sin 2(\beta - \alpha) \tan \beta + M_H^2(1 - 3 \cos 2(\beta - \alpha)) + M_h^2(1 + 3 \cos 2(\beta - \alpha)) - 4M_{H^\pm}^2 + 2v^2 \Lambda_3 \right]. \quad (3.2)$$

We see that in order to satisfy the unitarity constraint, a cancellation among the terms in the square bracket is required, and it turns out to be a severe upper bound on  $M_\Phi$ . In fact, we numerically find that  $M_\Phi$  has to be smaller than about 600 GeV in the WS scenario. On the contrary, in the A2HDM (right panel),  $\Lambda_2$  is the independent free parameter, so the large cancellation mentioned above is not needed. As a result, the limit on  $M_\Phi$  is much more relaxed as compared with the  $\mathbb{Z}_2$  symmetric case. However, very large  $M_\Phi$  is restricted as the couplings become too large as long as  $\cos(\beta - \alpha) \neq 0$ , see Eq. (2.10).

### 3.3 Flavor Constraints

We discuss constraints from flavor experiments. It is well known that the charged Higgs boson mediates in the  $B \rightarrow X_s \gamma$  decay process at the one-loop level, by which its mass  $M_{H^\pm}$  and parameters related to quark Yukawa couplings  $\zeta_u$  and  $\zeta_d$

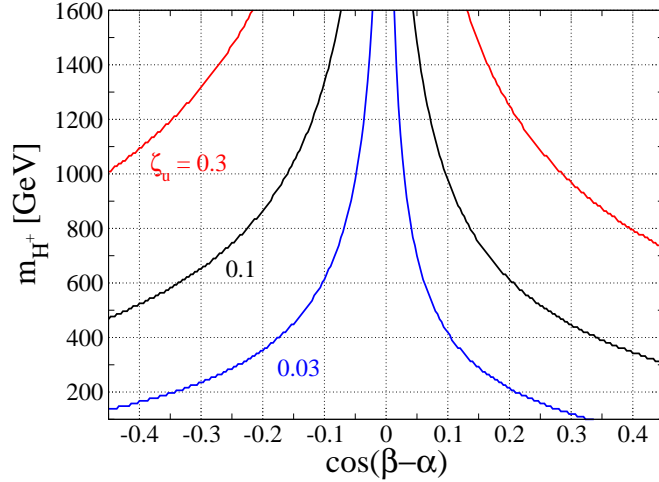


**Figure 5.** Constraint from  $B \rightarrow X_s \gamma$  for the case with the WS limit for down-type quarks. Regions below each curve is excluded at 95% CL.

are constrained. In the WS limit for down-type quarks,  $\zeta_d$  is determined by fixing  $\cos(\beta - \alpha)$ , so that the branching ratio of the  $B \rightarrow X_s \gamma$  decay is given in terms of  $M_{H^\pm}$ ,  $\zeta_u$  and  $\cos(\beta - \alpha)$ .

The current world average for the measurement of the branching ratio of  $B \rightarrow X_s \gamma$  is given by [59]

$$\mathcal{B}(B \rightarrow X_s \gamma) = (3.32 \pm 0.15) \times 10^{-4}. \quad (3.3)$$

We implement QCD and QED corrections at next-to-leading order (NLO) calculated in Refs. [60] and [61]. We apply the same SM inputs given in Ref. [62] to the numerical analysis, by which we obtain the SM prediction to be  $\mathcal{B}(B \rightarrow X_s \gamma) = 3.24 \times 10^{-4}$ . In Fig. 5, we show the lower limit on the value of  $M_{H^\pm}$  as a function of  $\cos(\beta - \alpha)$  for fixed values of  $\zeta_u$  to be 0.3 (red), 0.1 (black) and 0.03 (blue) from the data of  $B \rightarrow X_s \gamma$  decay. We see that stronger bounds on  $M_{H^\pm}$  are obtained for smaller values of  $|\cos(\beta - \alpha)|$  corresponding to larger  $|\zeta_d|$  due to the WS condition and/or larger values of  $\zeta_u$ , because the decay amplitude is enhanced by  $\zeta_u^2$  and/or  $\zeta_u \zeta_d$  terms. It is also seen that the case with  $\cos(\beta - \alpha) < 0$  ( $\zeta_d > 0$ ) gives a stronger bound on  $M_{H^\pm}$  as compared to that with  $\cos(\beta - \alpha) > 0$  ( $\zeta_d < 0$ ) for a fixed value of  $\zeta_u$ . This is because in the case with  $\zeta_d > 0$  the new physics contribution, proportional to  $\zeta_u \zeta_d$ , gives a destructive interference with the SM contribution, so it reduces the branching ratio. As we show above, the SM prediction is given below the central value, stronger limits are provided for  $\cos(\beta - \alpha) < 0$ . We note that in the Type-II case  $\zeta_u$  is fixed to be  $-1/\zeta_d (= \cot \beta)$ , so that the new physics contribution almost do not depend on  $\tan \beta$  for  $\tan \beta \gtrsim 2$ , and the current lower limit on  $M_{H^\pm}$  has been

taken to be around 800 GeV based on the calculation with next-to-NLO QCD [63]. We also note that the other flavor constraints, such as  $B_s \rightarrow \mu^+ \mu^-$  are typically much weaker than that from  $B \rightarrow X_s \gamma$  as long as we do not take extremely large value of  $|\zeta_e|$ , see e.g., Ref. [62].

## 4 Decays of Additional Higgs Bosons in RS & WS Scenarios

We compare decay branching ratios of the additional Higgs bosons in the WS and RS scenarios. Since the Type-II scenario has already been strongly constrained by LHC data and flavor observables [11], we here focus on the phenomenology in the Type-X 2HDM and the A2HDM with  $|\zeta_e| \gg |\zeta_{u/d}|$ . As we discussed in Sec. 3, in the WS scenario larger values of  $|\cos(\beta - \alpha)|$  are required for  $|\zeta_e| \gg 1$  as compared with the RS scenario, the phenomenology will be different from the RS region. Now, we present the difference in decays of the additional Higgs bosons in the RS and WS scenarios. For our phenomenological analysis, we assume that the additional Higgs bosons are degenerate in mass, i.e.,  $M_\Phi \equiv M_{H^\pm} (= M_A = M_H)$ .

For the  $H \rightarrow hh$  mode, the decay rate depends on the scalar trilinear coupling  $\lambda_{Hhh}$  defined as the coefficient of the  $Hhh$  vertex in the Lagrangian, which is given by

$$\begin{aligned} \lambda_{Hhh} &= -\frac{\cos(\beta - \alpha)}{2v} \left\{ M_H^2 - 4M_{H^\pm}^2 + \cos^2(\beta - \alpha) (6M_{H^\pm}^2 - 2M_h^2 - M_H^2) \right. \\ &\quad \left. + v^2 \left[ \frac{3}{2} \sin 2(\beta - \alpha) \Lambda_7 + (2 - 3 \cos^2(\beta - \alpha)) \Lambda_3 \right] \right\}, \\ &\simeq -\frac{\cos(\beta - \alpha)}{2v} \left\{ M_H^2 - 4M_{H^\pm}^2 + v^2 \left[ \frac{3}{2} \sin 2(\beta - \alpha) \Lambda_7 + 2\Lambda_3 \right] \right\}, \end{aligned} \quad (4.1)$$

where the last expression is valid for  $\sin(\beta - \alpha) \simeq 1$ . Thus, it depends on the additional parameters  $\Lambda_3$  and  $\Lambda_7$ , which do not appear in the other decay modes considered in this section. In the A2HDM, we take  $\Lambda_3 = \Lambda_7 = 0$  for a while, and later we show how the branching ratio of  $H \rightarrow hh$  is changed depending on the  $\Lambda_3$  and  $\Lambda_7$  parameters. In the Type-X 2HDM,  $\Lambda_7$  is determined by Eq. (2.13), while  $\Lambda_3$  is in principle free parameter, but its value is substantially determined by the unitarity bound. This can be seen from Eq. (3.2), i.e.,  $\Lambda_3$  is determined in such a way that terms in the square bracket of Eq. (3.2) vanish in order to maintain  $\Lambda_2$  to be order 1. We apply the above treatment for  $\Lambda_3$  and  $\Lambda_7$  to the following calculation.

In Fig. 6, we show the branching ratios of  $H$  (upper panels) and  $A$  (lower panels) in the Type-X 2HDM with  $\tan \beta = 10$  (solid curves) and 20 (dashed curves). The left and right panel respectively focuses on the RS and WS scenario, where the value of  $\cos(\beta - \alpha)$  is fixed to be 0.01 (almost the upper limit from the Higgs signal strength) and  $2/\tan \beta$  which gives  $\kappa_\tau = -1$  and  $\kappa_b \simeq \kappa_t \simeq 1$ . As expected, for the RS case, the  $H \rightarrow \tau\tau$  mode is dominant, and  $t\bar{t}$  can also be dominant for  $\tan \beta = 10$  and

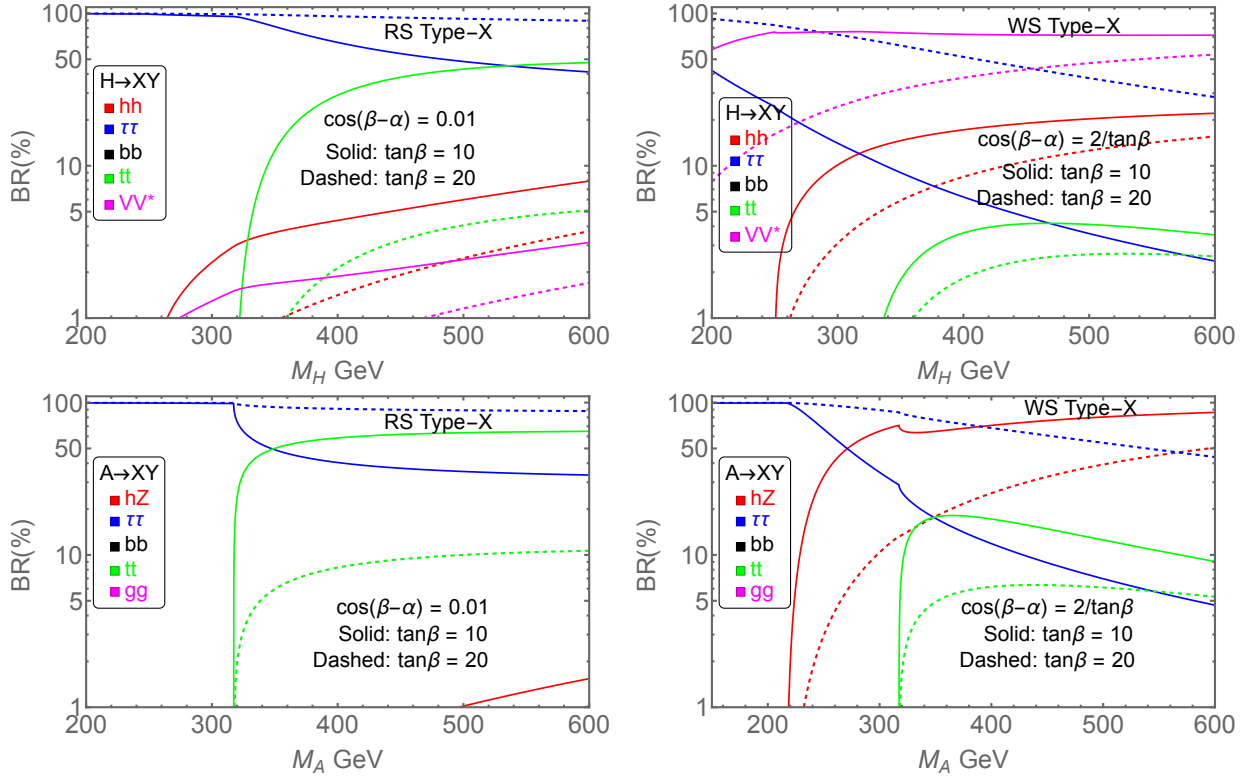


**Figure 6.** Comparison of branching ratios for the additional Higgs bosons ( $H$ : upper panels and  $A$ : lower panels) in the RS Type-X 2HDM with  $\cos(\beta - \alpha) = 0.01$  (left panels) and the WS Type-X 2HDM with  $\cos(\beta - \alpha) = 2/\tan\beta$  (right panels). The solid and dashed curves respectively show the case with  $\tan\beta = 10$  and 20.

$M_H > 2m_t$ . On the other hand, in the WS case,  $H \rightarrow VV$  ( $V = W^\pm, Z$ ) can be dominant instead of  $\tau\tau$ , particularly for the case with larger  $M_\Phi$ . In addition, the  $H \rightarrow hh$  decay can also be substantial. Similar behavior can be seen in the decay of  $A$ , but the  $A \rightarrow Zh$  can be dominant in the WS case as the  $VV$  and  $hh$  modes are forbidden for  $A$ . Therefore, it is clear that the decays into bosonic states become more important than the fermionic one in the WS scenario, which can be important to distinguish the WS scenario from the RS one.

In Fig. 7, we show the branching ratios for  $H$  (upper panels) and  $A$  (lower panels) in the A2HDM with  $\zeta_e = -20$ ,  $\zeta_d = 1$  and  $\Lambda_3 = \Lambda_7 = 0$ . The solid and dashed curves denote the case with  $\zeta_u = 0.1$  and 0.05, respectively. Again, the left (right) panel shows the result in the RS (WS) case, where we take  $\cos(\beta - \alpha) = 0.01$  ( $\cos(\beta - \alpha) = -2/\zeta_e$ ). These values mimic the Type-X Yukawa structure. Similar to the Type-X case, the decay modes into bosonic states are more important in the WS case as compared with the RS case. The difference between the WS scenario in the Type-X 2HDM and the A2HDM is seen in the  $H \rightarrow hh$  decay, which can be

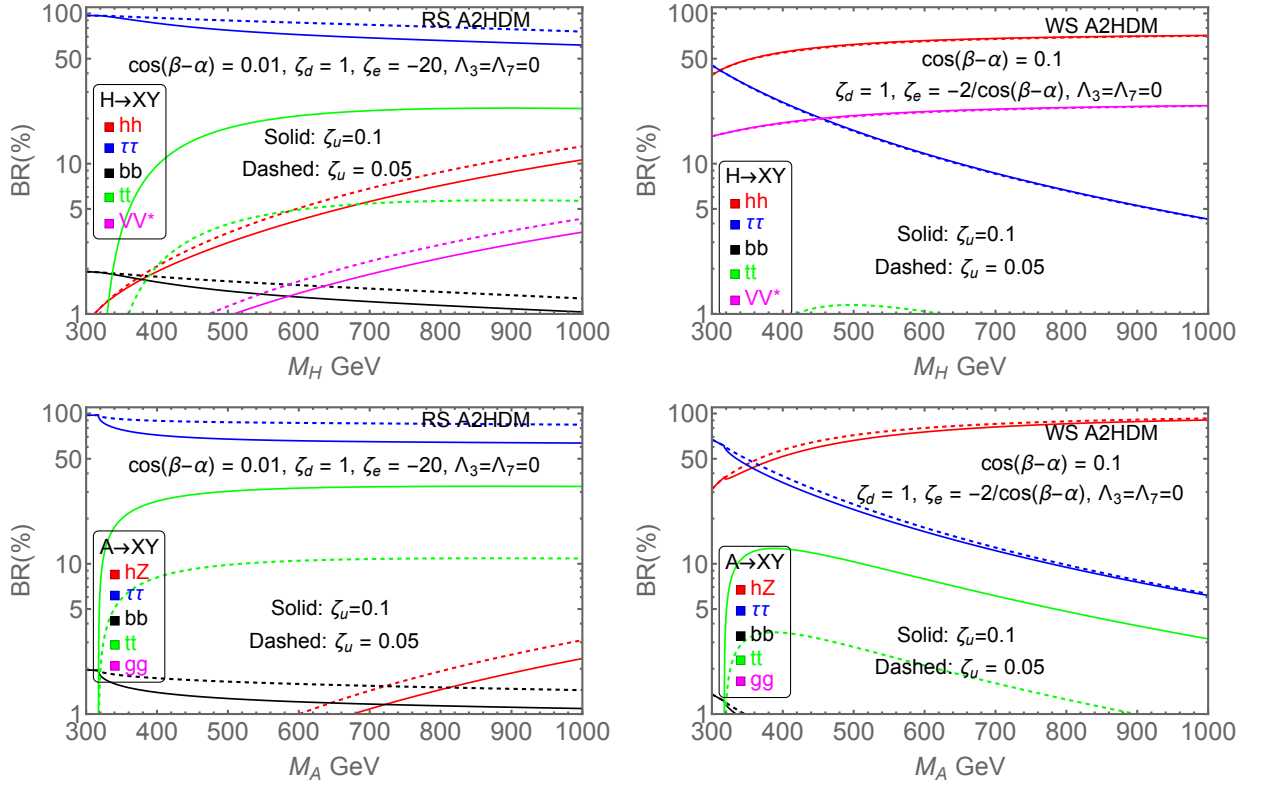


**Figure 7.** Comparison of branching ratios for the additional Higgs bosons ( $H$ : upper panels and  $A$ : lower panels) in the RS A2HDM with  $\cos(\beta - \alpha) = 0.01$  (left panels) and the WS A2HDM with  $\cos(\beta - \alpha) = 2/\tan\beta$  (right panels). We fix  $\zeta_d = 1$ ,  $\zeta_e = -20$  and  $\Lambda_3 = \Lambda_7 = 0$  for all the panels, while the solid and dashed curves respectively show the case with  $\zeta_u = 0.1$  and  $0.05$ .

more significant in the A2HDM than that in the Type-X 2HDM due to the freedom of the  $\Lambda_3$  and  $\Lambda_7$  parameters.

In Fig. 8, we show the contours of  $\text{BR}(H \rightarrow hh)$  on the  $\Lambda_3$ - $\Lambda_7$  plane (left) and the  $\Lambda_3$ - $M_H$  plane. We also depict the region excluded by theoretical constraints as the red-solid line. It is seen that a larger branching ratio is obtained for a smaller value of  $\Lambda_3$ , because it enhances the  $\lambda_{Hhh}$  coupling as seen in Eq. (4.1). On the other hand, the dependence of  $\Lambda_7$  on  $\text{BR}(H \rightarrow hh)$  is quite mild due to the suppression factor of  $\sin 2(\beta - \alpha)$ , see Eq. (4.1). The branching ratio can be significantly large values, e.g., about 60% at  $(\Lambda_3, \Lambda_7) = (-1, 0)$  with  $M_H = 300$  GeV. We note that the decay rate of  $H \rightarrow hh$  also strongly depends on the mass spectrum of the additional Higgs bosons as it can be seen in Eq. (4.1). For instance, if we take  $M_{H^\pm} - M_H = 50$  (100) GeV with  $M_H = 300$  GeV,  $M_A = M_{H^\pm}$  and  $\Lambda_3 = \Lambda_7 = 0$ , the branching ratio of  $H \rightarrow hh$  becomes about 60% (70%), which is allowed by the constraints from the

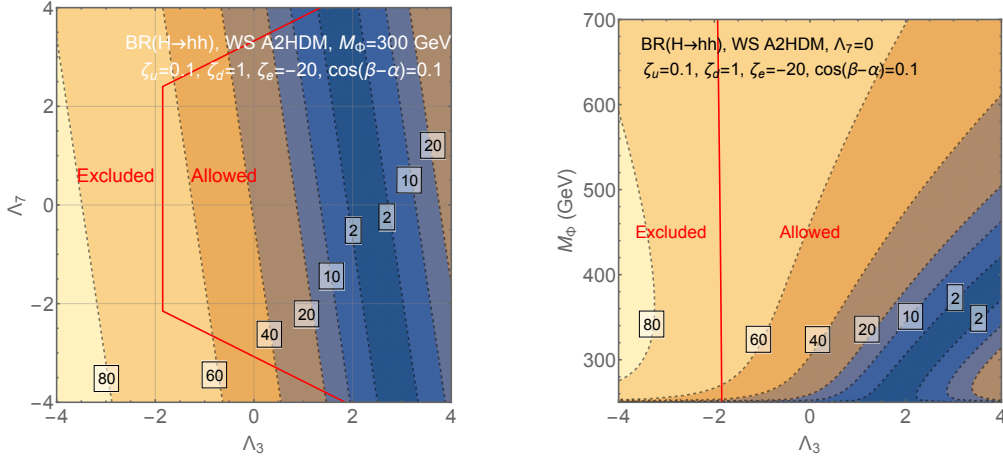


**Figure 8.** Contours of the branching ratio for  $H \rightarrow hh$  in percent on the  $\Lambda_3$ - $\Lambda_7$  plane (left) and the  $\Lambda_3$ - $M_H$  plane (right). Constraint from the vacuum stability of the scalar potential is indicated by the solid curves.

perturbative unitarity and vacuum stability as well as the electroweak  $T$  parameter due to the custodial symmetry in the Higgs potential [64].

## 5 Limits from Current LHC and HL-LHC

We discuss the parameter space giving the WS scenario in the Type-X 2HDM and the A2HDM, which is excluded by direct searches for additional Higgs bosons at the LHC Run-II experiment and is expected to be explored by the HL-LHC. In the following discussion, we take  $\Lambda_3 = \Lambda_7 = 0$ ,  $\zeta_u = 0.1$  and  $\zeta_d = 1$  in the A2HDM, and  $\Lambda_3$  is fixed so as to keep  $\Lambda_2$  to be order 1 in the Type-X 2HDM as we have done in the previous section.

The processes which are crucial to constrain the parameter space are the following:

$$pp \rightarrow A \rightarrow Zh, \quad pp \rightarrow A \rightarrow \tau\tau, \quad pp \rightarrow H \rightarrow hh, \quad pp \rightarrow H \rightarrow ZZ. \quad (5.1)$$

We apply the 95% CL upper limit on the cross section given at the LHC with the integrated luminosity of  $139 \text{ fb}^{-1}$  for the  $Zh$  [65],  $\tau\tau$  [66],  $hh$  [67] and  $ZZ$  [68] mode. Here, all the additional Higgs bosons are assumed to be produced via the gluon fusion process. We employ **SusHi** [69, 70] in order to estimate the production cross-section of the gluon fusion at NNLO. Since our scenarios are leptophilic, the  $b$  quark-associated production ( $b\bar{b}H$  and  $b\bar{b}A$ ) is negligible. Other relevant channels are  $pp \rightarrow H/A \rightarrow t\bar{t}$  [71] and the charged Higgs boson production from  $pp \rightarrow tH^\pm$  with the decays  $H^\pm \rightarrow tb$  [72],  $H^\pm \rightarrow \tau^\pm\nu$  [73] and  $H^\pm \rightarrow W^\pm h$  [74]. We, however, find that the limits from these channels are weaker than those from Eq. (5.1).



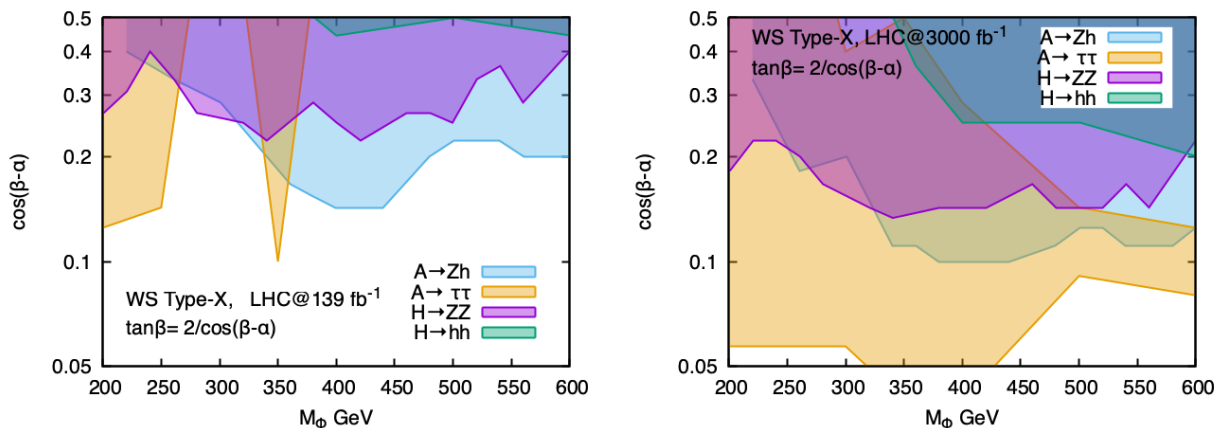


**Figure 9.** Shaded regions on the  $M_\Phi$ - $\cos(\beta - \alpha)$  plane are excluded at 95% CL from the direct searches at the current LHC (left) and the HL-LHC (right) in the Type-X 2HDM.

In Fig. 9, we show the parameter space in the Type-X 2HDM, which is excluded by the current LHC data (left) and is expected to be excluded by the HL-LHC with the integrated luminosity of  $3000 \text{ fb}^{-1}$  (right). In order to find out the limit expected at the HL-LHC, we calculate the signal cross section required for  $2\sigma$  significance assuming the same background cross section and the same 95% CL upper limit on the event number reported by the Run-II experiments. In this way, roughly  $\sqrt{139/3000} \simeq 0.22$  times smaller signal cross section with respect to that given at the Run-II experiment is excluded at the HL-LHC. The colored regions are excluded at 95% CL by the processes given in Eq. (5.1). As we have seen in Fig. 4, the upper limit on the mass is given to be about 600 GeV from the unitarity constraint, so that we show the region up to 600 GeV. We see that most of the region with  $\cos(\beta - \alpha) \gtrsim 0.2$  is excluded by the combination of the various constraints from the direct searches, while that with smaller values of  $\cos(\beta - \alpha)$  is allowed, because the production cross section is suppressed by  $\cot^2 \beta$  which is now fixed by the WS condition, i.e.,  $\tan \beta \simeq 2/\cos(\beta - \alpha)$ . At the HL-LHC, the region expected to be excluded is enlarged up to  $\cos(\beta - \alpha) \gtrsim 0.1$ .

In the A2HDM, the LHC limits strongly depend on the value of  $\zeta_u$  as the production of the neutral Higgs bosons via gluon fusion is directly proportional to  $\zeta_u^2$ . In Fig. 10, we show the LHC bounds for  $\zeta_u = 0.1$ . We see that the region with smaller  $\cos(\beta - \alpha)$  is excluded mainly by the  $A \rightarrow \tau\tau$  mode, because the decay rate of  $A \rightarrow \tau\tau$  ( $A \rightarrow Zh$  and  $H \rightarrow hh$ ) is proportional to  $\zeta_e^2 \simeq [2/\cos(\beta - \alpha)]^2$ . On the other hand, the case with larger  $\cos(\beta - \alpha)$  is excluded by the  $A \rightarrow Zh$  and  $H \rightarrow hh$  modes, because the decay rates of these modes are suppressed by  $\cos^2(\beta - \alpha)$ . Thus, these two channels are complementary with each other. We note that the limits from

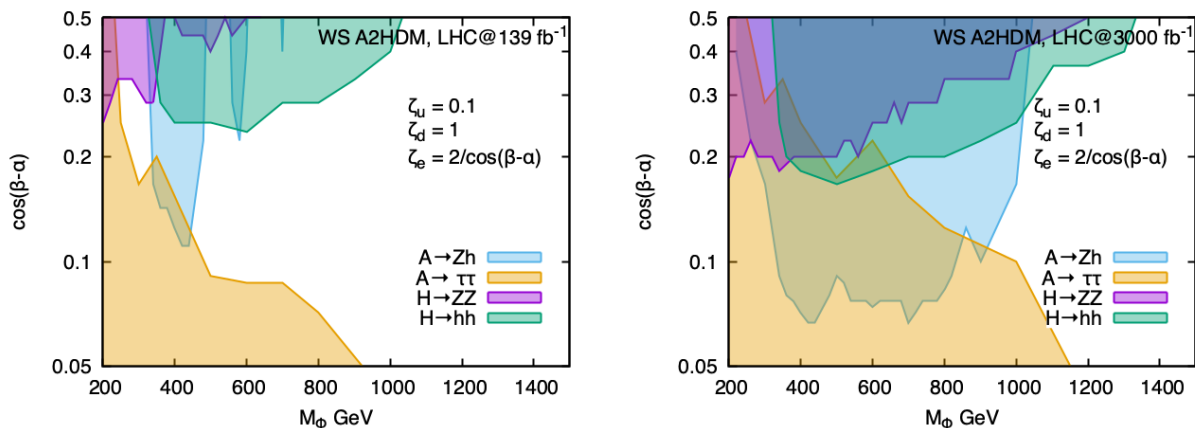


**Figure 10.** Shaded regions on the  $M_\Phi$ - $\cos(\beta - \alpha)$  plane are excluded at 95% CL from the direct searches at the current LHC (left) and the HL-LHC (right) in the A2HDM.

the searches for  $A$  vanish for  $\zeta_u < 0.05$ . In the right panel, we show the prospect of the direct searches at the HL-LHC. As expected, a broader parameter space will be explored if  $\zeta_u$  is large.

## 6 Multi-Higgs Signatures in the WS Scenario

We discuss how we can distinguish the WS scenario from the RS one at the LHC. As discussed in Sec. 4, the additional Higgs bosons predominantly decay into bosonic channels including the discovered Higgs boson  $h$  in the WS scenario as compared to the RS case. Thus, we expect that a larger number of events with multi-Higgs final states can be obtained in the WS scenario than that in the RS case.

In order to clarify this, we consider a pair production of the additional Higgs bosons via gauge interactions [75–80], which is quite useful to extract the structure of the Yukawa couplings, because its cross section is simply determined by the masses of the additional Higgs bosons in the Higgs alignment limit. We here consider the following processes:

$$pp \rightarrow Z^* \rightarrow AH, \quad pp \rightarrow W^{\pm*} \rightarrow H^\pm H / H^\pm A, \quad (6.1)$$

with the succeeding decays

$$A \rightarrow Zh, \quad H \rightarrow hh / WW / ZZ, \quad \text{and} \quad H^\pm \rightarrow Wh. \quad (6.2)$$

In the near alignment regime, i.e.,  $\cos(\beta - \alpha) \simeq 0$ , the cross section of the above processes slightly reduces as they are proportional to  $\sin^2(\beta - \alpha)$  except for the  $AH^\pm$

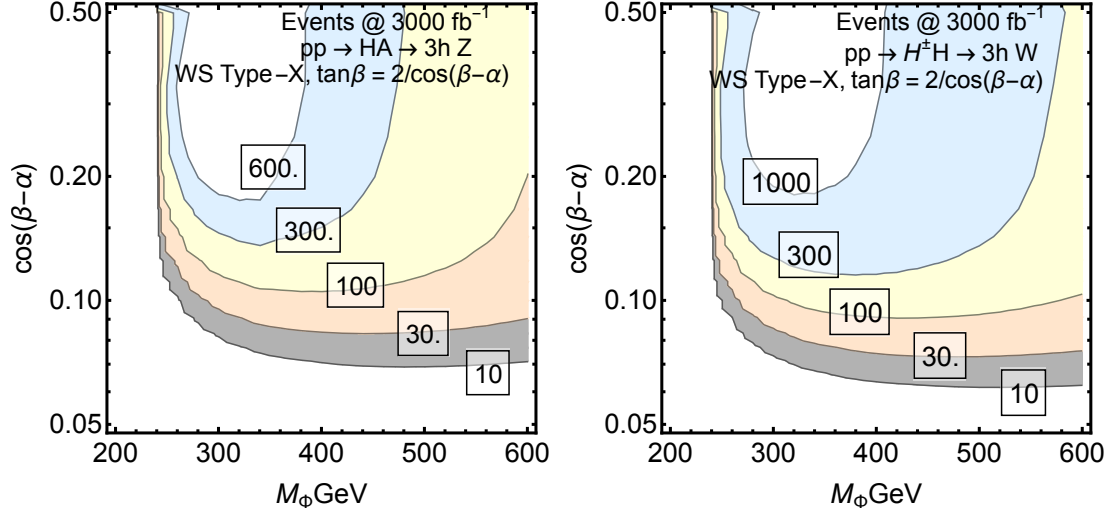


**Figure 11.** New possible search channels and number of events in various multi Higgs final states at HL-LHC in the Type-X 2HDM

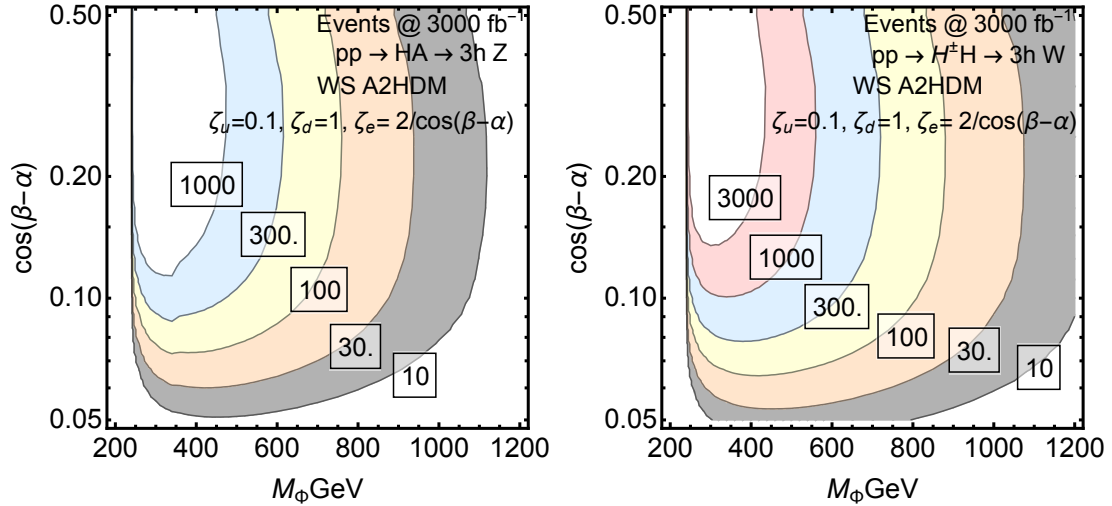


**Figure 12.** New possible search channels and number of events in various multi Higgs final states at HL-LHC in the A2HDM

production. To estimate the production cross-section we use `FeynRules` [81, 82] and `MadGraph5_aMC@NLO` [83, 84]. We also use a uniform K-factor of 1.34 [79] to incorporate higher-order QCD corrections. We note that the Yukawa induced productions discussed in the previous section are, of course, useful to see the difference between the RS and WS scenarios. However, these production cross sections strongly depend on the structure of the Yukawa coupling. In particular, when we consider a case with large  $\tan\beta$  in the Type-X 2HDM or that with smaller  $\zeta_u$  in the A2HDM, these pro-

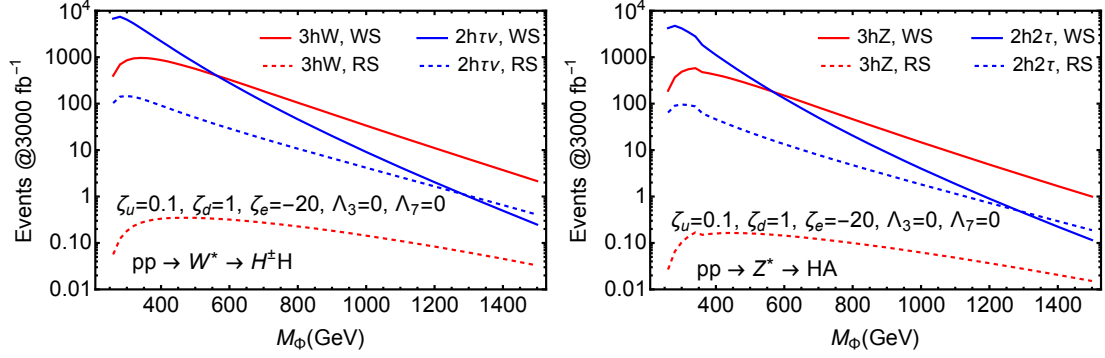


**Figure 13.** Comparison of the number of events in the multi-Higgs final states for the RS (dashed) and WS(solid) cases.

cesses cannot be used because the cross section is highly suppressed by the smaller top Yukawa coupling for  $H$  and  $A$ .

We estimate the number of events in various multi-Higgs final states with an integrated luminosity of  $3000 \text{ fb}^{-1}$ . For simplicity, we assume a degenerate mass spectrum, i.e.,  $M_\Phi \equiv M_{H^\pm} (= M_A = M_H)$  as a conservative analysis. We note that for the case with a mass difference  $M_{H^\pm} > M_H$  and  $M_{H^\pm} = M_A$ , the decay branching ratio of  $H \rightarrow hh$  increases as discussed in Sec. 4. In addition, a portion of the branching ratios of  $A \rightarrow Zh$  and  $H^\pm \rightarrow W^\pm h$  is replaced by those of  $A \rightarrow Z^{(*)}H$  and  $H^\pm \rightarrow W^{\pm(*)}H$ , which eventually can provide a larger number of  $h$  in the final state due to the succeeding decay of  $H \rightarrow hh$ .

In Fig. 11, we show the contour plot for the number of events with three Higgs bosons, i.e.,  $hhhZ$  (left) and  $hhhW$  (right) as a function of  $M_\Phi$  and  $\cos(\beta - \alpha)$  in the WS Type-X 2HDM. For  $\cos(\beta - \alpha) \simeq 0.15$  which is just below the current upper limit by LHC data,  $\mathcal{O}(100)$  events are expected for the  $hhhZ$  mode. For the  $hhhW$  mode, almost double the number of events is expected as compared with the  $hhhZ$  mode. We also show the number of events for two Higgs final states in Appendix B. Similarly in Fig. 12, we show the number of events for the three Higgs final states in the WS A2HDM.

Finally in Fig. 13, we compare the expected number of multi-Higgs events in the A2HDM with the WS and RS scenarios at the HL-LHC. It is clear that the event number for the  $3h + W(Z)$  final states in the WS case is about three orders of magnitude larger than that in the RS case, and almost no event can be seen in the RS case. We have also estimated the  $2h + \tau\nu(\tau)$  final state for which the RS event yield is non zero, but remain much smaller than WS case unless the scalars are very heavy. Hence we have considered multi Higgs final state in this section. Therefore, the measurement of the multi-Higgs final state can be an important probe for testing the WS scenario.

Before closing this section, let us remark that dedicated signal and background analyses must be required in order to clarify the significance of these multi-Higgs events, in which we can consider various final states depending on the decay of the Higgs boson  $h$ . Such a dedicated phenomenological analysis is beyond the scope of the present study.

## 7 Conclusion

We have studied the scenario with WS Yukawa couplings for the discovered Higgs boson with the mass of 125 GeV in the Type-X 2HDM and the A2HDM. The WS  $ht\bar{t}$  coupling has already been ruled out due to the constraint from measurements of the  $h \rightarrow \gamma\gamma$  decay at the LHC, while WS couplings for down-type quarks and charged leptons are still possible. We have focused on the WS scenario for charged leptons in the Type-X 2HDM and the A2HDM under theoretical constraints such as vacuum stability, perturbative unitarity and perturbativity as well as the bounds from flavor data, Higgs signal strengths and direct searches at the LHC. It has been shown that in the WS scenario, the additional Higgs bosons tend to mainly decay into bosonic states, e.g.,  $H \rightarrow hh/WW/ZZ$ ,  $A \rightarrow Zh$  and  $H^\pm \rightarrow W^\pm h$  as compared with those in the RS scenario. We have shown that the existing LHC searches thoroughly explore the WS Type-X scenario mainly via  $H \rightarrow hh$ ,  $A \rightarrow Zh$  and  $A \rightarrow \tau\tau$  channels. For the A2HDM case, the LHC limit from the existing searches strongly depends on the up-type alignment parameter ( $\zeta_u$ ). For instance, for  $\zeta_u = 0.1$ , the masses of the additional Higgs bosons up to about 1 TeV can be explored at the HL-LHC. Finally, we have proposed to look for a final state of multi-Higgs bosons in association with gauge bosons via the electroweak production of the additional Higgs bosons. Such multi-Higgs signatures at the LHC will be an undisputable indication of the WS nature of Yukawa couplings.

## Acknowledgments

This work was supported in part by JSPS KAKENHI Grants No. 20H00160, No. 22F21324 and by Grant-in-Aid for Early-Career Scientists, No. 19K14714.

## A Higgs measurement data

In Sec. 3, we have performed the  $\chi^2$  analysis in order to constrain the parameter space of the 2HDMs, in which we have used the current measurements of the Higgs signal strengths for various channels at the LHC. For the production, we have taken into account the gluon fusion process (ggF), the vector boson fusion process (VBF), the vector boson associated process ( $Vh$ ) and the top quark associated process ( $t\bar{t}h$ ).

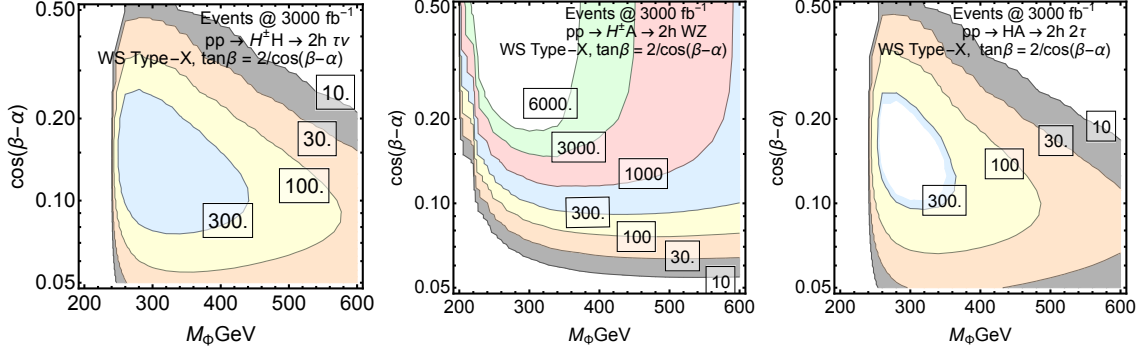


**Figure 14.** New possible search channels and number of events in various multi Higgs final state at HL-LHC in the WS Type-X 2HDM.

For the decay, we have taken into account the  $h \rightarrow \gamma\gamma$ ,  $h \rightarrow WW^*$ ,  $h \rightarrow ZZ^*$ ,  $h \rightarrow \tau\tau$  and  $h \rightarrow b\bar{b}$  modes. In Tab. 1, we summarize the current data that we used in our  $\chi^2$  analysis.

|             | Exp. | $\gamma\gamma$       | $WW^*$              | $ZZ^*$              | $\tau\tau$           | $b\bar{b}$          |
|-------------|------|----------------------|---------------------|---------------------|----------------------|---------------------|
| ggF         | A    | $1.03 \pm 0.11$ [1]  | $1.08 \pm 0.19$ [1] | $0.94 \pm 0.11$ [1] | $0.95 \pm 0.30$ [85] |                     |
|             | C    | $1.07 \pm 0.12$ [86] | $1.28 \pm 0.20$ [2] | $0.98 \pm 0.12$ [2] | $0.97 \pm 0.19$ [87] | $2.45 \pm 2.45$ [2] |
| VBF         | A    | $1.31 \pm 0.25$ [1]  | $0.62 \pm 0.35$ [1] | $1.25 \pm 0.45$ [1] | $0.89 \pm 0.18$ [85] | $3.0 \pm 1.6$ [1]   |
|             | C    | $1.04 \pm 0.33$ [86] | $0.63 \pm 0.63$ [2] | $0.57 \pm 0.41$ [2] | $0.68 \pm 0.24$ [87] | $1.3 \pm 1.1$ [88]  |
| $Vh$        | A    | $1.32 \pm 0.32$ [1]  | $3.2 \pm 4.3$ [1]   | $1.53 \pm 1.01$ [1] | $0.95 \pm 0.58$ [85] | $1.02 \pm 0.18$ [1] |
|             | C    | $1.34 \pm 0.35$ [86] | $1.00 \pm 1.28$ [2] | $1.10 \pm 0.85$ [2] | $1.80 \pm 0.44$ [87] | $1.05 \pm 0.25$ [2] |
| $t\bar{t}h$ | A    | $0.9 \pm 0.25$ [1]   |                     |                     | $1.53 \pm 1.41$ [85] | $0.79 \pm 0.60$ [1] |
|             | C    | $1.35 \pm 0.34$ [86] | $0.93 \pm 0.45$ [2] |                     | $0.8 \pm 0.7$ [2]    | $1.13 \pm 0.32$ [2] |

**Table 1.** Current data for the measurements of the Higgs signal strengths at the LHC. Here, “A” and “C” denote ATLAS and CMS, respectively.

## B Number of events for two Higgs final states

We show the expected number of events for the two Higgs final states from the decay of the additional Higgs bosons. In Figs. 14 and 15, we show the contour plots for the number of events in the WS Type-X 2HDM and the WS A2HDM, respectively.

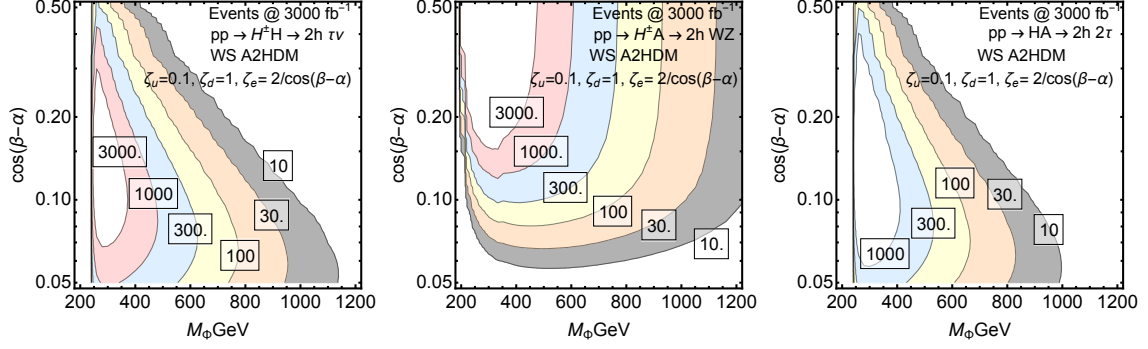


**Figure 15.** New possible search channels and number of events in various multi Higgs final state at HL-LHC in the WS A2HDM.

## References

- [1] ATLAS collaboration, *A combination of measurements of Higgs boson production and decay using up to 139 fb<sup>-1</sup> of proton–proton collision data at  $\sqrt{s} = 13$  TeV collected with the ATLAS experiment*, .
- [2] CMS collaboration, *Combined Higgs boson production and decay measurements with up to 137 fb<sup>-1</sup> of proton–proton collision data at  $\sqrt{s} = 13$  TeV*, .
- [3] LHC HIGGS CROSS SECTION WORKING GROUP collaboration, *Handbook of LHC Higgs Cross Sections: 3. Higgs Properties*, [1307.1347](#).
- [4] I. F. Ginzburg, M. Krawczyk and P. Osland, *Resolving SM like scenarios via Higgs boson production at a photon collider. 1. 2HDM versus SM*, [hep-ph/0101208](#).
- [5] P. M. Ferreira, J. F. Gunion, H. E. Haber and R. Santos, *Probing wrong-sign Yukawa couplings at the LHC and a future linear collider*, *Phys. Rev. D* **89** (2014) 115003 [[1403.4736](#)].
- [6] B. Dumont, J. F. Gunion, Y. Jiang and S. Kraml, *Constraints on and future prospects for Two-Higgs-Doublet Models in light of the LHC Higgs signal*, *Phys. Rev. D* **90** (2014) 035021 [[1405.3584](#)].
- [7] D. Fontes, J. C. Romão and J. a. P. Silva, *A reappraisal of the wrong-sign  $h\bar{b}b$  coupling and the study of  $h \rightarrow Z\gamma$* , *Phys. Rev. D* **90** (2014) 015021 [[1406.6080](#)].
- [8] A. Biswas and A. Lahiri, *Alignment, reverse alignment, and wrong sign Yukawa couplings in two Higgs doublet models*, *Phys. Rev. D* **93** (2016) 115017 [[1511.07159](#)].
- [9] T. Modak, J. C. Romão, S. Sadhukhan, J. a. P. Silva and R. Srivastava, *Constraining wrong-sign  $h\bar{b}b$  couplings with  $h \rightarrow \Upsilon\gamma$* , *Phys. Rev. D* **94** (2016) 075017 [[1607.07876](#)].
- [10] P. M. Ferreira, S. Liebler and J. Wittbrodt,  *$pp \rightarrow A \rightarrow Zh$  and the wrong-sign limit of the two-Higgs-doublet model*, *Phys. Rev. D* **97** (2018) 055008 [[1711.00024](#)].



- [11] W. Su, *Probing loop effects in wrong-sign Yukawa coupling region of Type-II 2HDM*, *Eur. Phys. J. C* **81** (2021) 404 [[1910.06269](#)].
- [12] X.-F. Han and H.-X. Wang, *Revisiting wrong sign Yukawa coupling of type II two-Higgs-doublet model in light of recent LHC data*, *Chin. Phys. C* **44** (2020) 073101 [[2003.06170](#)].
- [13] M. Raju, J. P. Saha, D. Das and A. Kundu, *Double Higgs boson production as an exclusive probe for a sequential fourth generation with wrong-sign Yukawa couplings*, *Phys. Rev. D* **101** (2020) 055036 [[2001.05280](#)].
- [14] T. Abe, R. Sato and K. Yagyu, *Lepton-specific two Higgs doublet model as a solution of muon  $g - 2$  anomaly*, *JHEP* **07** (2015) 064 [[1504.07059](#)].
- [15] A. Cherchiglia, D. Stöckinger and H. Stöckinger-Kim, *Muon  $g-2$  in the 2HDM: maximum results and detailed phenomenology*, *Phys. Rev. D* **98** (2018) 035001 [[1711.11567](#)].
- [16] L. Wang, J. M. Yang, M. Zhang and Y. Zhang, *Revisiting lepton-specific 2HDM in light of muon  $g - 2$  anomaly*, *Phys. Lett. B* **788** (2019) 519 [[1809.05857](#)].
- [17] J. Cao, P. Wan, L. Wu and J. M. Yang, *Lepton-Specific Two-Higgs Doublet Model: Experimental Constraints and Implication on Higgs Phenomenology*, *Phys. Rev.* **D80** (2009) 071701 [[0909.5148](#)].
- [18] A. Broggio, E. J. Chun, M. Passera, K. M. Patel and S. K. Vempati, *Limiting two-Higgs-doublet models*, *JHEP* **11** (2014) 058 [[1409.3199](#)].
- [19] V. Ilisie, *New Barr-Zee contributions to  $(g - 2)_\mu$  in two-Higgs-doublet models*, *JHEP* **04** (2015) 077 [[1502.04199](#)].
- [20] ATLAS collaboration, *Search for Higgs bosons decaying to  $aa$  in the  $\mu\mu\tau\tau$  final state in  $pp$  collisions at  $\sqrt{s} = 8$  TeV with the ATLAS experiment*, *Phys. Rev. D* **92** (2015) 052002 [[1505.01609](#)].
- [21] CMS collaboration, *Search for light bosons in decays of the 125 GeV Higgs boson in proton-proton collisions at  $\sqrt{s} = 8$  TeV*, *JHEP* **10** (2017) 076 [[1701.02032](#)].
- [22] ATLAS collaboration, *Search for Higgs boson decays to beyond-the-Standard-Model light bosons in four-lepton events with the ATLAS detector at  $\sqrt{s} = 13$  TeV*, *JHEP* **06** (2018) 166 [[1802.03388](#)].
- [23] CMS collaboration, *Search for an exotic decay of the Higgs boson to a pair of light pseudoscalars in the final state of two muons and two  $\tau$  leptons in proton-proton collisions at  $\sqrt{s} = 13$  TeV*, *JHEP* **11** (2018) 018 [[1805.04865](#)].
- [24] CMS collaboration, *Search for light pseudoscalar boson pairs produced from decays of the 125 GeV Higgs boson in final states with two muons and two nearby tracks in  $pp$  collisions at  $\sqrt{s} = 13$  TeV*, *Phys. Lett. B* **800** (2020) 135087 [[1907.07235](#)].
- [25] CMS collaboration, *Search for a light pseudoscalar Higgs boson in the boosted  $\mu\mu\tau\tau$  final state in proton-proton collisions at  $\sqrt{s} = 13$  TeV*, *JHEP* **08** (2020) 139 [[2005.08694](#)].



- [26] E. J. Chun and J. Kim, *Leptonic Precision Test of Leptophilic Two-Higgs-Doublet Model*, *JHEP* **07** (2016) 110 [[1605.06298](#)].
- [27] E. J. Chun, S. Dwivedi, T. Mondal and B. Mukhopadhyaya, *Reconstructing a light pseudoscalar in the Type-X Two Higgs Doublet Model*, *Phys. Lett. B* **774** (2017) 20 [[1707.07928](#)].
- [28] N. Ghosh and J. Lahiri, *Generalized 2HDM with wrong-sign lepton-Yukawa coupling, in light of  $g_\mu - 2$  and lepton flavor violation at the future LHC*, *Eur. Phys. J. C* **81** (2021) 1074 [[2103.10632](#)].
- [29] J. Kim, *Compatibility of muon  $g-2$ ,  $W$  mass anomaly in type-X 2HDM*, *Phys. Lett. B* **832** (2022) 137220 [[2205.01437](#)].
- [30] A. Pich and P. Tuzon, *Yukawa Alignment in the Two-Higgs-Doublet Model*, *Phys. Rev. D* **80** (2009) 091702 [[0908.1554](#)].
- [31] S. Kanemura, M. Kubota and K. Yagyu, *Aligned CP-violating Higgs sector canceling the electric dipole moment*, *JHEP* **08** (2020) 026 [[2004.03943](#)].
- [32] S. Kanemura, M. Kubota and K. Yagyu, *Testing aligned CP-violating Higgs sector at future lepton colliders*, *JHEP* **04** (2021) 144 [[2101.03702](#)].
- [33] K. Enomoto, S. Kanemura and Y. Mura, *Electroweak baryogenesis in aligned two Higgs doublet models*, *JHEP* **01** (2022) 104 [[2111.13079](#)].
- [34] K. Enomoto, S. Kanemura and Y. Mura, *New benchmark scenarios of electroweak baryogenesis in aligned two Higgs double models*, *JHEP* **09** (2022) 121 [[2207.00060](#)].
- [35] O. Eberhardt, A. P. n. Martínez and A. Pich, *Global fits in the Aligned Two-Higgs-Doublet model*, *JHEP* **05** (2021) 005 [[2012.09200](#)].
- [36] S. Kanemura, T. Kubota and E. Takasugi, *Lee-Quigg-Thacker bounds for Higgs boson masses in a two doublet model*, *Phys. Lett. B* **313** (1993) 155 [[hep-ph/9303263](#)].
- [37] A. G. Akeroyd, A. Arhrib and E.-M. Naimi, *Note on tree level unitarity in the general two Higgs doublet model*, *Phys. Lett. B* **490** (2000) 119 [[hep-ph/0006035](#)].
- [38] J. Horejsi and M. Kladiva, *Tree-unitarity bounds for THDM Higgs masses revisited*, *Eur. Phys. J. C* **46** (2006) 81 [[hep-ph/0510154](#)].
- [39] I. F. Ginzburg and I. P. Ivanov, *Tree-level unitarity constraints in the most general 2HDM*, *Phys. Rev. D* **72** (2005) 115010 [[hep-ph/0508020](#)].
- [40] S. Kanemura and K. Yagyu, *Unitarity bound in the most general two Higgs doublet model*, *Phys. Lett. B* **751** (2015) 289 [[1509.06060](#)].
- [41] N. G. Deshpande and E. Ma, *Pattern of Symmetry Breaking with Two Higgs Doublets*, *Phys. Rev. D* **18** (1978) 2574.
- [42] S. Nie and M. Sher, *Vacuum stability bounds in the two Higgs doublet model*, *Phys. Lett. B* **449** (1999) 89 [[hep-ph/9811234](#)].

- [43] S. Kanemura, T. Kasai and Y. Okada, *Mass bounds of the lightest CP even Higgs boson in the two Higgs doublet model*, *Phys. Lett. B* **471** (1999) 182 [[hep-ph/9903289](#)].
- [44] S. Kanemura, M. Kikuchi and K. Yagyu, *Next-to-leading order corrections to decays of the heavier CP-even Higgs boson in the two Higgs doublet model*, *Nucl. Phys. B* **983** (2022) 115906 [[2203.08337](#)].
- [45] M. Aiko, S. Kanemura and K. Sakurai, *Radiative corrections to decay branching ratios of the CP-odd Higgs boson in two Higgs doublet models*, [2207.01032](#).
- [46] M. Aiko, S. Kanemura and K. Sakurai, *Radiative corrections to decays of charged Higgs bosons in two Higgs doublet models*, *Nucl. Phys. B* **973** (2021) 115581 [[2108.11868](#)].
- [47] J. F. Gunion, H. E. Haber, G. L. Kane and S. Dawson, *The Higgs Hunter's Guide*, vol. 80. 2000.
- [48] A. Djouadi, *The Anatomy of electro-weak symmetry breaking. II. The Higgs bosons in the minimal supersymmetric model*, *Phys. Rept.* **459** (2008) 1 [[hep-ph/0503173](#)].
- [49] G. C. Branco, P. M. Ferreira, L. Lavoura, M. N. Rebelo, M. Sher and J. P. Silva, *Theory and phenomenology of two-Higgs-doublet models*, *Phys. Rept.* **516** (2012) 1 [[1106.0034](#)].
- [50] F. J. Botella and J. P. Silva, *Jarlskog - like invariants for theories with scalars and fermions*, *Phys. Rev. D* **51** (1995) 3870 [[hep-ph/9411288](#)].
- [51] S. Davidson and H. E. Haber, *Basis-independent methods for the two-Higgs-doublet model*, *Phys. Rev. D* **72** (2005) 035004 [[hep-ph/0504050](#)].
- [52] S. Gori, H. E. Haber and E. Santos, *High scale flavor alignment in two-Higgs doublet models and its phenomenology*, *JHEP* **06** (2017) 110 [[1703.05873](#)].
- [53] V. Barger, H. E. Logan and G. Shaughnessy, *Identifying extended Higgs models at the LHC*, *Phys. Rev. D* **79** (2009) 115018 [[0902.0170](#)].
- [54] Y. Grossman, *Phenomenology of models with more than two Higgs doublets*, *Nucl. Phys.* **B426** (1994) 355 [[hep-ph/9401311](#)].
- [55] M. Aoki, S. Kanemura, K. Tsumura and K. Yagyu, *Models of Yukawa interaction in the two Higgs doublet model, and their collider phenomenology*, *Phys. Rev. D* **80** (2009) 015017 [[0902.4665](#)].
- [56] A. Dainese, M. Mangano, A. B. Meyer, A. Nisati, G. Salam and M. A. Vesterinen, eds., *Report on the Physics at the HL-LHC, and Perspectives for the HE-LHC*, vol. 7/2019 of *CERN Yellow Reports: Monographs*. CERN, Geneva, Switzerland, 2019, [10.23731/CYRM-2019-007](#).
- [57] S. Kanemura, K. Tsumura, K. Yagyu and H. Yokoya, *Fingerprinting nonminimal Higgs sectors*, *Phys. Rev. D* **90** (2014) 075001 [[1406.3294](#)].
- [58] S. Kanemura, M. Kikuchi and K. Yagyu, *Fingerprinting the extended Higgs sector*

- using one-loop corrected Higgs boson couplings and future precision measurements, *Nucl. Phys. B* **896** (2015) 80 [[1502.07716](#)].
- [59] HFLAV collaboration, *Averages of  $b$ -hadron,  $c$ -hadron, and  $\tau$ -lepton properties as of 2018*, *Eur. Phys. J. C* **81** (2021) 226 [[1909.12524](#)].
- [60] F. Borzumati and C. Greub, *2HDMs predictions for anti- $B \rightarrow X(s)$  gamma in NLO QCD*, *Phys. Rev. D* **58** (1998) 074004 [[hep-ph/9802391](#)].
- [61] A. L. Kagan and M. Neubert, *QCD anatomy of  $B \rightarrow X(s)$  gamma decays*, *Eur. Phys. J. C* **7** (1999) 5 [[hep-ph/9805303](#)].
- [62] S. Kanemura, M. Takeuchi and K. Yagyu, *Probing double-aligned two-Higgs-doublet models at the LHC*, *Phys. Rev. D* **105** (2022) 115001 [[2112.13679](#)].
- [63] M. Misiak and M. Steinhauser, *Weak radiative decays of the  $B$  meson and bounds on  $M_{H^\pm}$  in the Two-Higgs-Doublet Model*, *Eur. Phys. J. C* **77** (2017) 201 [[1702.04571](#)].
- [64] A. Pomarol and R. Vega, *Constraints on CP violation in the Higgs sector from the rho parameter*, *Nucl. Phys. B* **413** (1994) 3 [[hep-ph/9305272](#)].
- [65] ATLAS collaboration, *Search for heavy resonances decaying into a  $Z$  or  $W$  boson and a Higgs boson in final states with leptons and  $b$ -jets in  $139 \text{ fb}^{-1}$  of  $pp$  collisions at  $\sqrt{s} = 13 \text{ TeV}$  with the ATLAS detector*, [2207.00230](#).
- [66] ATLAS collaboration, *Search for heavy Higgs bosons decaying into two tau leptons with the ATLAS detector using  $pp$  collisions at  $\sqrt{s} = 13 \text{ TeV}$* , *Phys. Rev. Lett.* **125** (2020) 051801 [[2002.12223](#)].
- [67] ATLAS collaboration, *Search for resonant pair production of Higgs bosons in the  $b\bar{b}b\bar{b}$  final state using  $pp$  collisions at  $\sqrt{s} = 13 \text{ TeV}$  with the ATLAS detector*, *Phys. Rev. D* **105** (2022) 092002 [[2202.07288](#)].
- [68] ATLAS collaboration, *Search for heavy resonances decaying into a pair of  $Z$  bosons in the  $\ell^+\ell^-\ell'^+\ell'^-$  and  $\ell^+\ell^-\nu\bar{\nu}$  final states using  $139 \text{ fb}^{-1}$  of proton-proton collisions at  $\sqrt{s} = 13 \text{ TeV}$  with the ATLAS detector*, *Eur. Phys. J. C* **81** (2021) 332 [[2009.14791](#)].
- [69] R. V. Harlander, S. Liebler and H. Mantler, *SusHi: A program for the calculation of Higgs production in gluon fusion and bottom-quark annihilation in the Standard Model and the MSSM*, *Comput. Phys. Commun.* **184** (2013) 1605 [[1212.3249](#)].
- [70] R. V. Harlander, S. Liebler and H. Mantler, *SusHi Bento: Beyond NNLO and the heavy-top limit*, *Comput. Phys. Commun.* **212** (2017) 239 [[1605.03190](#)].
- [71] ATLAS collaboration, *Search for heavy particles decaying into top-quark pairs using lepton-plus-jets events in proton-proton collisions at  $\sqrt{s} = 13 \text{ TeV}$  with the ATLAS detector*, *Eur. Phys. J. C* **78** (2018) 565 [[1804.10823](#)].
- [72] ATLAS collaboration, *Search for charged Higgs bosons decaying into a top quark and a bottom quark at  $\sqrt{s} = 13 \text{ TeV}$  with the ATLAS detector*, *JHEP* **06** (2021) 145 [[2102.10076](#)].

- [73] ATLAS collaboration, *Search for charged Higgs bosons decaying via  $H^\pm \rightarrow \tau^\pm \nu_\tau$  in the  $\tau$ +jets and  $\tau$ +lepton final states with  $36 \text{ fb}^{-1}$  of pp collision data recorded at  $\sqrt{s} = 13 \text{ TeV}$  with the ATLAS experiment*, *JHEP* **09** (2018) 139 [[1807.07915](#)].
- [74] CMS collaboration, *Search for a charged Higgs boson decaying into a heavy neutral Higgs boson and a W boson in proton-proton collisions at  $\sqrt{s} = 13 \text{ TeV}$* , [2207.01046](#).
- [75] S. Kanemura and C. P. Yuan, *Testing supersymmetry in the associated production of CP odd and charged Higgs bosons*, *Phys. Lett. B* **530** (2002) 188 [[hep-ph/0112165](#)].
- [76] Q.-H. Cao, S. Kanemura and C. P. Yuan, *Associated production of CP odd and charged Higgs bosons at hadron colliders*, *Phys. Rev. D* **69** (2004) 075008 [[hep-ph/0311083](#)].
- [77] A. Belyaev, Q.-H. Cao, D. Nomura, K. Tobe and C. P. Yuan, *Light MSSM Higgs boson scenario and its test at hadron colliders*, *Phys. Rev. Lett.* **100** (2008) 061801 [[hep-ph/0609079](#)].
- [78] E. J. Chun, S. Dwivedi, T. Mondal, B. Mukhopadhyaya and S. K. Rai, *Reconstructing heavy Higgs boson masses in a type X two-Higgs-doublet model with a light pseudoscalar particle*, *Phys. Rev. D* **98** (2018) 075008 [[1807.05379](#)].
- [79] H. Bahl, T. Stefaniak and J. Wittbrodt, *The forgotten channels: charged Higgs boson decays to a  $W^\pm$  and a non-SM-like Higgs boson*, *JHEP* **06** (2021) 183 [[2103.07484](#)].
- [80] T. Mondal and P. Sanyal, *Same sign trilepton as signature of charged Higgs in two Higgs doublet model*, *JHEP* **05** (2022) 040 [[2109.05682](#)].
- [81] N. D. Christensen and C. Duhr, *FeynRules - Feynman rules made easy*, *Comput. Phys. Commun.* **180** (2009) 1614 [[0806.4194](#)].
- [82] A. Alloul, N. D. Christensen, C. Degrande, C. Duhr and B. Fuks, *FeynRules 2.0 - A complete toolbox for tree-level phenomenology*, *Comput. Phys. Commun.* **185** (2014) 2250 [[1310.1921](#)].
- [83] J. Alwall, M. Herquet, F. Maltoni, O. Mattelaer and T. Stelzer, *MadGraph 5 : Going Beyond*, *JHEP* **06** (2011) 128 [[1106.0522](#)].
- [84] J. Alwall, R. Frederix, S. Frixione, V. Hirschi, F. Maltoni, O. Mattelaer et al., *The automated computation of tree-level and next-to-leading order differential cross sections, and their matching to parton shower simulations*, *JHEP* **07** (2014) 079 [[1405.0301](#)].
- [85] ATLAS collaboration, *Measurements of Higgs boson production cross-sections in the  $H \rightarrow \tau^+ \tau^-$  decay channel in pp collisions at  $\sqrt{s} = 13 \text{ TeV}$  with the ATLAS detector*, *JHEP* **08** (2022) 175 [[2201.08269](#)].
- [86] CMS collaboration, *Measurements of Higgs boson production cross sections and couplings in the diphoton decay channel at  $\sqrt{s} = 13 \text{ TeV}$* , *JHEP* **07** (2021) 027 [[2103.06956](#)].

- [87] CMS collaboration, *Measurements of Higgs boson production in the decay channel with a pair of  $\tau$  leptons in proton-proton collisions at  $\sqrt{s} = 13$  TeV*, [2204.12957](#).
- [88] CMS COLLABORATION collaboration, *Search for the standard model Higgs boson produced through vector boson fusion and decaying to  $bb$  with proton-proton collisions at  $\sqrt{s} = 13$  TeV*, tech. rep., CERN, Geneva, 2016.